

1 Do fungi look like macroparasites? Quantifying the patterns and  
2 mechanisms of aggregation for host-fungal parasite relationships

3  
4 **Authors:** Sarah A.R. Schrock<sup>1</sup>, Jason C. Walsman<sup>2</sup>, Joseph DeMarchi<sup>1</sup>, Emily H. LeSage<sup>3</sup>, Michel E.B.  
5 Ohmer<sup>4</sup>, Louise A. Rollins-Smith<sup>5,6</sup>, Cheryl J. Briggs<sup>2</sup>, Corinne L. Richards-Zawacki<sup>7</sup>, Douglas C. Woodhams<sup>8</sup>,  
6 Roland A. Knapp<sup>9,10</sup>, Thomas C. Smith<sup>9,10</sup>, Célio F.B. Haddad<sup>11</sup>, C. Guilherme Becker<sup>12,13</sup>, Pieter T.J.  
7 Johnson<sup>14</sup>, Mark Q. Wilber<sup>1</sup>

8 **Author affiliations:**

9 <sup>1</sup>School of Natural Resources, University of Tennessee Institute of Agriculture, Knoxville, TN, USA

10 <sup>2</sup>Ecology, Evolution, and Marine Biology, University of California, Santa Barbara, CA, USA

11 <sup>3</sup>Biology Department, Skidmore College, Saratoga Springs, NY, USA

12 <sup>4</sup>Department of Biology, University of Mississippi, University, MS, USA

13 <sup>5</sup>Department of Pathology, Microbiology, and Immunology, Vanderbilt University School of Medicine, Nashville,  
14 TN, USA

15 <sup>6</sup>Department of Biological Sciences, Vanderbilt University, Nashville, TN, USA

16 <sup>7</sup>Department of Biological Sciences and Pymatuning Laboratory of Ecology, University of Pittsburgh, PA,  
17 USA

18 <sup>8</sup>Department of Biology, University of Massachusetts, Boston, MA, USA

19 <sup>9</sup>Sierra Nevada Aquatic Research Laboratory, University of California, Mammoth Lakes, CA, USA

20 <sup>10</sup>Earth Research Institute, University of California, Santa Barbara, CA, USA

21 <sup>11</sup>Department of Biodiversity and Aquaculture Center (CAUNESP), Universidade Estadual Paulista, Rio  
22 Claro, SP, Brazil

23 <sup>12</sup>Department of Biology, The Pennsylvania State University, University Park, PA, USA

24 <sup>13</sup>One Health Microbiome Center, Center for Infectious Disease Dynamics, Ecology Institute, Huck Institutes  
25 of the Life Sciences, The Pennsylvania State University, University Park, PA, USA

26 <sup>14</sup>Ecology and Evolutionary Biology, University of Colorado Boulder, Boulder, CO, USA

27

28 **Corresponding author:** Sarah A.R. Schrock, School of Natural Resources, University of Tennessee Insti-  
29 tute of Agriculture, Knoxville, TN, USA.

30 [sschroc2@tennessee.edu](mailto:sschroc2@tennessee.edu)

## 31 Abstract

32 Most hosts contain few parasites, whereas few hosts contain many. This pattern, known as aggregation, is  
33 well-documented in macroparasites where parasite intensity distribution among hosts affects host-parasite  
34 dynamics. Infection intensity also drives fungal disease dynamics, but we lack a basic understanding of host-  
35 fungal aggregation patterns, how they compare to macroparasites, and if they reflect biological processes.  
36 To address these gaps, we characterized aggregation of the fungal pathogen *Batrachochytrium dendrobatidis*  
37 (Bd) in amphibian hosts. Utilizing the slope of Taylor's Power Law, we found Bd intensity distributions  
38 were more aggregated than macroparasites, conforming closely to lognormal distributions. We observed that  
39 Bd aggregation patterns are strongly correlated with known biological processes operating in amphibian  
40 populations, such as epizootological phase—invasion, post-invasion, and enzootic—and intensity-dependent  
41 disease mortality. Using intensity-dependent mathematical models, we found evidence of evolution of host  
42 resistance based on aggregation shifts in systems persisting with Bd following disease-induced declines. Our  
43 results show that Bd aggregation is highly conserved across disparate systems and is distinct from aggrega-  
44 tion patterns in macroparasites, and contains signatures of potential biological processes of amphibian-Bd  
45 systems. Our work lays a foundation to unite host-fungal dynamics under a common theoretical framework  
46 and inform future modeling approaches that may elucidate host-fungus interactions.

## 47 Introduction

48 One of the few general laws of parasitology is that many hosts have few parasites, and few hosts have many  
49 parasites [1]. Known as "aggregation", this pattern has important implications for the dynamics of host-  
50 parasite systems and our ability to infer the dominant processes operating within them [2; 3; 4]. For example,  
51 some macroparasites can cause intensity-dependent parasite-induced mortality, and the severity of this pro-  
52 cess can be reflected in the intensity distribution of parasites across hosts [5; 6]. In wildlife-macroparasite  
53 systems, such as nematodes, trematodes, and ectoparasitic arthropods, the nature of aggregation has been  
54 extensively quantified [7; 8]: the distribution of macroparasites among hosts is often well-described by a  
55 negative binomial distribution, and variance-to-mean relationships are significantly different from Poisson  
56 expectations. While we have long been able to quantify the intensity of macroparasites (e.g., by counting  
57 parasites following dissection), we can now also quantify infection intensity of microparasites through the  
58 broad application of modern molecular techniques. Microparasites are organisms such as bacteria, viruses,  
59 protozoa, and fungi that have high replication rates within a host and often induce host immune responses [9].  
60 While studies on microparasites now regularly report quantitative measures of infection (e.g., viral titers or

61 fungal intensity within a host), we have few baseline expectations regarding what the intensity distributions  
62 of microparasites look like and the mechanisms shaping them.

63 Here, we focus on fungal parasites. Fungal parasites are a global threat to wildlife populations [10]: e.g.,  
64 *Batrachochytrium dendrobatidis* (Bd), *B. salamandrivorans*, *Ophidiomyces ophiodiicola*, and *Pseudogymnoas-*  
65 *cus destructans* have led to dramatic declines and extinctions in hundreds of wildlife species [11; 12; 13; 14].  
66 Like macroparasites, animals infected with fungal parasites suffer intensity-dependent parasite-induced mor-  
67 tality [15; 16]. This means that accounting for the distribution of fungal parasite intensity within a population  
68 is critical for predicting population-level outcomes following fungal invasion [17; 18]. However, despite mod-  
69 eling work increasingly accounting for fungal infection intensity [17; 19], we still lack a general understanding  
70 of the quantitative patterns of aggregation in host-fungal parasite systems. Quantifying these patterns is  
71 important because i) different levels of aggregation change system dynamics and can significantly affect  
72 model predictions [20; 21] and ii) patterns in fungal intensity distributions may reflect dominant mechanistic  
73 processes structuring the host-parasite system [22]. The latter is particularly important for parasites like  
74 Bd where cryptic disease-induced mortality may drive ongoing declines [23], but detecting these declines is  
75 difficult. Aggregation patterns in fungal intensity distributions could potentially provide a mechanism to  
76 detect signatures of disease-induced mortality, as has been done in host-macroparasite systems [6].

77 Describing the distribution of fungal parasite intensity requires a different statistical and conceptual  
78 treatment than traditional macroparasite models. Macroparasite infection intensity is typically described by  
79 parasite counts—in other words, how many parasites are found within a host, ranging from zero to some  
80 large number. As such, macroparasite counts are discrete and can be described by distributions such a  
81 Poisson or negative binomial distribution [8]. In contrast, fungal parasite intensity is typically quantified  
82 by molecular approaches such as quantitative PCR [qPCR; 24]. The qPCR technique measures the amount  
83 of a specific DNA sequence in a sample by amplifying the sequence while simultaneously detecting and  
84 quantifying the fluorescence of the product in real-time as the reaction proceeds. Because the amount of  
85 fluorescence generated is directly proportional to the amount of starting DNA, qPCR values correlate with  
86 fungal intensity. The resulting measurement of "infection intensity" is a continuous variable ranging from  
87 zero to some arbitrarily large number.

88 Using infection intensity as a continuous quantity computed by qPCR presents two methodological chal-  
89 lenges. First, qPCR measures of infection intensity are subject to substantial measurement error [25; 26].  
90 Measurement error can come when the sample of infection intensity is collected (e.g., the skin of amphibians  
91 infected with Bd are swabbed) or when the sample is processed with qPCR [26]. For example, the qPCR  
92 process often fails to detect very low quantities of genetic material and can miss low levels of infection [27; 26].  
93 Generally, increasing the noise in a sample due to measurement error might decrease our ability to detect

94 biological signals. Thus, we might expect measurement error to play a more significant role in affecting the  
95 patterns of aggregation in fungal intensity distributions than typical macroparasite distributions, obscuring  
96 mechanistic signatures of host-parasite processes on fungal intensity distributions.

97 Second, discrete distributions that are typically used to describe macroparasite counts are not technically  
98 applicable to continuous molecular infection intensity data. In amphibian-Bd systems, there has been some  
99 previous discussion on reasonable assumptions for the distribution of infection intensity [particularly with  
100 regards to the random component of generalized linear models; 25] and how approximating a continuous  
101 random variable with a discrete random variable [e.g., using a negative binomial distribution to describe  
102 infection intensity 25] can affect the conclusions one draws. However, there has been no systematic exami-  
103 nation of the distribution that most consistently describes observed amphibian-Bd distributions or parasitic  
104 fungal distributions more broadly. As we continue to develop models for predicting the dynamics of fungal  
105 outbreaks, a systematic quantification of the nature of fungal intensity distributions can help direct these  
106 modeling efforts, as it has done in traditional macroparasite systems [7; 8].

107 In addition to these statistical differences, there are key biological differences between fungal parasites  
108 and macroparasites that may affect observed patterns of aggregation. Fungal parasites grow within/on a host  
109 leading to increases in infection intensity. Typically (though not always), macroparasite infections increase  
110 in intensity through "immigration processes" rather than "birth processes"—hosts repeatedly encounter  
111 parasites in the environment which leads to an accumulation of parasites. Birth processes such as the within-  
112 host reproduction of parasites are known to increase the aggregation of macroparasite distributions [28; 29].  
113 An initial expectation might be that fungal distributions are typically more aggregated than macroparasite  
114 distributions. However, this prediction is complicated by the speed and mode of transmission of fungal  
115 parasites, which can be faster than many macroparasites. For example, Bd can complete its life cycle in four  
116 to ten days, whereas a trematode parasite with multiple intermediate hosts might take months to complete  
117 its life cycle [30; 31]. This could lead to faster spread, more homogenization, and lower levels of aggregation  
118 for fungal parasites like Bd compared to macroparasites.

119 Here, we utilized 56,912 skin swab samples from 93 amphibian species to ask two main questions: (1)  
120 What is the general structure of these fungal intensity distributions, and (2) do they reflect biological pro-  
121 cesses? First, we examined whether we see aggregation in host-Bd systems, how these patterns compare  
122 to those of macroparasites, and what statistical distribution best describes these fungal intensity distribu-  
123 tions. We hypothesized that i) fungal distributions will be aggregated, ii) they will show higher levels of  
124 aggregation than most macroparasite distributions, and iii) they will generally conform to a lognormal dis-  
125 tribution. Our prediction of a lognormal distribution stems from theoretical work showing that lognormal  
126 distributions robustly describe population densities subject to demographic and environmental stochastic-

127 ity, as well as measurement error [32]. To address our second question, we compared aggregation patterns  
128 among amphibian-Bd systems in different epizootological states (e.g., invasion, post-invasion, and enzootic)  
129 to see if they reflect underlying biological processes. To complement data analysis, we employed an integral  
130 projection model to gain insight into the possible mechanisms driving the observed aggregation patterns.  
131 Given intensity-dependent disease dynamics in amphibian-Bd systems, we expected reduced aggregation  
132 in populations experiencing significant disease-induced mortality, such as those in post-invasion, epizootic  
133 states. Similarly, we expected disease-induced mortality to be a critical model parameter in reproducing  
134 these patterns.

## 135 **Materials and Methods**

### 136 **Amphibian-Bd infection intensity data**

137 We analyzed four datasets of Bd infection intensities (henceforth "intensity" or "load") obtained from am-  
138 phibian skin swabs collected in the field. Bd loads were obtained through DNA extraction and qPCR, which  
139 detects the number of genomic equivalents or ITS1 copy number of Bd on amphibian skin. These procedures  
140 were standardized within but not across datasets. As such, it is important to note that our analysis does  
141 not aim to compare absolute values of fungal intensities across datasets or even among disparate sites within  
142 datasets. Variations in techniques between labs and calculations of Bd intensity (e.g. multiplying by different  
143 scaling factors) as well as differences in ITS copy numbers for different strains of Bd in different sites [e.g.,  
144 33] could make comparisons challenging. Instead, we use measures of aggregation (described below) that  
145 are scale invariant, thus providing robust measures to analyze aggregation patterns. However, if individuals  
146 of the same species of amphibian in the same site in the same season are co-infected with different strains  
147 of Bd that vary in their ITS1 copy number [e.g., 34], then the aggregation metrics we estimate could suffer  
148 bias.

149 The first dataset we included was from Brazil (henceforth the Brazil dataset) which contained 4,365  
150 swabs from 41 amphibian species collected primarily within the state of São Paulo (see Fig. S1 for general  
151 locations of research sites for all datasets). Our second dataset comes from the East Bay region of California  
152 (henceforth the East Bay dataset) and contains 10,490 swabs from 11 host species. The third dataset  
153 contains 12,457 Bd swabs from amphibians collected from 2016-2019 on 43 amphibian species across 31  
154 research sites in four states—Louisiana, Pennsylvania, Tennessee, and Vermont. Although collected across a  
155 wide geographical range, swabs from this study were all processed at a centralized location using a consistent  
156 methodology. Therefore, we will refer to this dataset broadly as the Eastern US dataset. Our final dataset is

157 from the Sierra Nevada mountains of California (henceforth the Sierra dataset) and contains 29,600 samples  
158 collected from mountain yellow-legged frogs (MYL frogs; composed of sister species *Rana muscosa* and *Rana*  
159 *sierrae*) at high elevation lakes, ponds, and wetlands.

160 Samples within each dataset were grouped based on host species, life stage (larva, subadult, or adult),  
161 research site, season (Brazil: Wet or Dry; East Bay and Sierra: Summer; Eastern US: winter, spring, summer,  
162 or fall), and year (see Table S1 for more detailed composition of each dataset). Moving forward, we will refer  
163 to a particular combination of species, life stage, research site, season, and year as a "group". Examining  
164 specific "groups" allows us to quantify the patterns of Bd aggregation in a biologically relevant temporal  
165 period at a particular location. In total, the Brazil dataset had 109 candidate groups for analysis, East Bay  
166 had 714, Eastern US had 391, and the Sierra had 647.

## 167 **Question 1a: Are fungal intensity distributions aggregated and how do these** 168 **compare with aggregation patterns in macroparasite systems?**

169 To address this question, we analyzed aggregation in the fungal intensity distributions using Taylor's Power  
170 Law (TPL) which relates the log mean and log variance in fungal intensity, calculated for each group. This  
171 metric allows for direct comparison to the macroparasite literature. Specifically, we focused on the slope  
172 of TPL as a metric of aggregation, where a greater slope indicates greater aggregation [28; 3]. Across all  
173 datasets, we only included groups with at least three infected individuals, yielding 961 groups across all four  
174 datasets (Table S1).

175 We first fit a linear regression to the log mean vs. log variance relationship for each of the four datasets and  
176 calculated the slope. We compared the slopes to the empirical relationship previously seen in macroparasite  
177 populations (slope=1.55, 95% Confidence Interval: [1.48,1.62]) [7], as well as a Poisson distribution (mean-  
178 variance slope equal to 1), which is generally considered the null distribution in many host-macroparasite  
179 studies [2]. However, the continuous nature of Bd load data also suggests considering the alternative null  
180 with a TPL slope of 2. A baseline of TPL slope of 2 has been used to describe the aggregation of free-living  
181 organisms in space and time [35; 36]. Moreover, given our expectation of a lognormal distribution of Bd  
182 intensity across hosts, we would expect a TPL slope of 2 based on the simple definitions of the mean and  
183 variance for a lognormal distribution. Note that for this analysis, the log mean and the log variance for each  
184 group was computed using both infected and uninfected individuals, consistent with macroparasite studies.

185 Second, to explore variability in the slope of TPL across the 36 species with sufficient sampling, we  
186 ran a linear mixed effect model (i.e., Gaussian error) with random effects of amphibian species and sub-  
187 region on the intercept and slope. Specifically, the model we fit was  $\log(\text{variance}) \sim \log(\text{mean}) + (1 +$

188  $\log(\text{mean})|\text{subregion}) + (1 + \log(\text{mean})|\text{species})$ , where subregion was a factor with the following levels: East  
189 Bay, Sierra, Pennsylvania, Tennessee, Vermont, Louisiana, and Brazil. We then examined the species-specific  
190 TPL slopes and compared them to the macroparasite slope from Shaw and Dobson (1995) [7].

### 191 **Question 1b: What distribution best describes fungal intensity distributions?**

192 To characterize the shape of fungal intensity distributions conditional on infection, we considered continuous  
193 distributions of nonnegative real numbers: gamma, exponential, lognormal, and Weibull. We did not consider  
194 Poisson and negative binomial distributions because fungal intensity, as assessed using qPCR, is a continuous  
195 measure. Although qPCR results can be transformed into integer values and analyzed using standard  
196 generalized linear models [37], we opted to keep the data on the continuous scale, consistent with previous  
197 models [19]. Each of the continuous distributions can capture a strong right skew in intensity distributions,  
198 consistent with canonical patterns in host-macroparasite systems. The gamma distribution is the continuous  
199 analog to the negative binomial distribution, a distribution that describes many macroparasite populations  
200 [8]. Similarly, the exponential is a special case of the gamma distribution that is represented by only one  
201 parameter and is analogous to the discrete geometric distribution which has been proposed as a potential null  
202 distribution in host-macroparasite systems [38; 39]. Lognormal distributions are found throughout natural  
203 systems empirically and theoretically [32] and are representative of nonnegative metrics with relatively low  
204 means but large variance. Finally, we considered the Weibull distribution which is typically used to model  
205 "time-to-failure" or survival analyses but has been used to describe macroparasite aggregation data [40].

206 For this analysis, we only considered groups with at least 10 infected individuals to ensure we had power  
207 to distinguish between competing distributions. This resulted in 525 groups. We used the `fitdistrplus`  
208 package in R to fit exponential, lognormal, Weibull, and gamma distributions using maximum likelihood  
209 estimation (MLE) or moment matching estimation, if the MLE model would not converge. We compared  
210 Akaike information criterion (AIC) values across distributions to find the best predictive model, assuming  
211 no notable difference in performance when AIC values were within  $\pm 2$ .

### 212 **Question 2: Do patterns of aggregation in Bd intensity reflect biological pro-** 213 **cesses, such that there are quantifiable differences in aggregation between epi-** 214 **zoological states?**

215 To address this question, we used a metric that can be applied to a single group (unlike TPL) known  
216 as Poulin's Discrepancy Index, or simply Poulin's D [41; 4]. Poulin's D is bounded from 0 to 1 and is a  
217 proportional measure of the difference between an observed distribution and a uniform distribution. A higher

218 value indicates greater discrepancy from a uniform distribution and is suggestive of higher aggregation. The  
219 equation for Poulin’s D is  $D = (\sum_{i=1}^n \sum_{j=1}^n |x_i - x_j|) / (2n^2 \bar{x})$ , where  $x$  is the fungal load of host  $i$  or  $j$ ,  $n$   
220 is the total number of hosts, and  $\bar{x} = \sum_{i=1}^n x_i / n$  [we use the equation given in 42, which is the Gini index].  
221 We also calculated the coefficient of variation (CV) on the natural scale and other related metrics— $\log_{10}$ -  
222 transformed CV on the natural scale and CV on the  $\log_{10}$  scale—which should provide comparable results  
223 to Poulin’s D [42]. We calculated CV on the  $\log_{10}$ -transformed data to determine if trends remained similar  
224 on different scales. When calculating our aggregation metrics, we excluded uninfected individuals to remove  
225 the effect of prevalence on the observed patterns. We only included groups that had at least two infected  
226 individuals—the minimum number for a meaningful value of our metrics. We also explored only including  
227 groups with a minimum of 10 infected individuals, and our results were unchanged.

228 For this question, we focused on the Sierra dataset. Of the datasets used in this study, the Sierra dataset  
229 is unique because for many southern populations in the Sierra Nevada, we know when Bd invaded, when  
230 epizootics ensued, and when populations declined [43; 15; 44]. Moreover, for more northern populations,  
231 such as those in Yosemite National Park, we know that populations are past the invasion-epizootic-declining  
232 phase and are persisting enzootically with Bd [45; 17]. Thus, we have three clearly definable epizootological  
233 phases for MYL-Bd populations in the Sierra Nevada: 1) invasion stage [when Bd prevalence is less than  
234 50% in a population; 46] 2) post-invasion phase (consisting of epizootic host declines or recent declines)  
235 and 3) enzootic phase (Bd invaded before the early 2000’s and amphibian populations are persisting in the  
236 presence of Bd). Moreover, from targeted field surveys and laboratory experiments, we know that there is  
237 strong intensity-dependent mortality in MYL frogs [15; 19]. If patterns of Bd aggregation contain information  
238 about intensity-dependent mortality, we would expect a notable reduction in Bd aggregation for higher mean  
239 infection intensity in MYL frog populations [3]. In other words, mortality in highly infected individuals would  
240 effectively reduce the tail of the right-skewed distribution characteristic of aggregated populations, thereby  
241 decreasing aggregation.

242 To explore signatures of epizootological phase on Bd aggregation, we first plotted each metric—Poulin’s D,  
243 CV, log CV, and CV of log-scale data—against mean  $\log_{10}$ -transformed Bd intensity and asked whether pop-  
244 ulations in known epizootological phases clustered in mean intensity-aggregation space (henceforth intensity-  
245 aggregation space) and whether there were notable reductions in aggregation at high infection intensities  
246 (note that epizootological phases were determined independently of aggregation or mean infection intensity).  
247 We used beta regression [4] to test for a quadratic effect of mean infection intensity on aggregation metrics,  
248 where a strong quadratic effect is indicative of aggregation being reduced at high infection intensity.

249 Finally, to better understand how mechanisms such as intensity-dependent mortality and epizootological  
250 phase could theoretically affect patterns of aggregation in host-fungal systems, we adapted an Integral

251 Projection Model (IPM) that has been previously developed for amphibian-Bd systems [19]. In short,  
252 IPMs provide an approach for modeling intensity-dependent infection dynamics of host-fungal interactions  
253 by specifically modeling the entire distribution of fungal intensities within a population (see supplementary  
254 material for more detail). Hosts are born uninfected, and in the absence of disease, the host population grows  
255 logistically toward a carrying capacity. In one time step of the model, hosts may become infected by encounter  
256 with environmental pathogens and gain some initial log number of parasites (infection load). Parasites grow  
257 within hosts, with some stochasticity, toward a within-host carrying capacity. In each time step, infected  
258 hosts have a probability of recovery from infection and a probability of survival, both of which decline  
259 with infection load. Infected hosts shed parasites back into the environment proportional to the number of  
260 parasites they currently hold. We simulated disease invasion for one year to represent the effects of disease  
261 spread without host evolution. We then added simulations where we included multiple host genotypes with  
262 different traits to simulate evolution over 30 years (a relevant timescale for the MYL-Bd system). Specifically,  
263 we focused on host evolution of resistance that lowers pathogen growth rate, an important mechanism in  
264 the MYL-Bd system [45; 37]. We performed simulations at parameter values from laboratory experiments  
265 for the MYL-Bd system (see Table S2 in supplementary material) and then explored how varying certain  
266 parameters impacted the intensity-aggregation patterns in our simulations. We calculated the same four  
267 aggregation metrics in our simulations as were calculated from field data to determine intensity-aggregation  
268 patterns. We did this to investigate the patterns that could emerge in intensity-aggregation space for the  
269 different metrics and if they are indicative of specific biological mechanisms.

## 270 Results

### 271 **Question 1a: Are fungal intensity distributions aggregated and how do these** 272 **compare with aggregation patterns in macroparasite systems?**

273 Based on TPL, Bd showed a greater degree of aggregation compared to macroparasites (Fig. 1). The slopes  
274 of TPL across the groups for each dataset ranged between 1.90, 95% CI [1.86-1.94] (Sierra) and 2.06, 95%  
275 CI [1.99-2.12] (Brazil), which are all significantly higher than the macroparasite slope given by Shaw and  
276 Dobson (1.55, 95% CI [1.48-1.62])[7] (Fig. 1). Therefore, the variance of Bd infection intensity increases to  
277 a greater degree with respect to average fungal load than many macroparasites.

278 We examined how the slopes of TPL varied among amphibian species and life stages. While we found  
279 significant variation in the slope of TPL among species (including slope as a random effect among species  
280 yielded a better predictive model than a model without a species-level random effect of slope:  $\Delta\text{AIC}=13.6$ ),

281 Bd was more aggregated on all amphibian species than for many macroparasites (see Fig. S2). We found  
282 a similar pattern across host life stage, showing slopes greater than that of macroparasites. However, the  
283 slopes for each life stage were statistically distinct: larval (1.85, 95% CI [1.82-1.89]), subadult (1.93, 95% CI  
284 [1.91-1.95]), and adult (2.01, 95% CI [1.98-2.04]).

### 285 **Question 1b: What distribution best describes fungal intensity distributions?**

286 Of the distributions that we fit to the Bd-positive data, the lognormal model consistently performed better  
287 than the others, as determined by comparing AIC scores (Fig. 2). Assuming models perform equally well if  
288 AIC scores are within 2 units of each other, over half of the groups (57.3%) were well-described by multiple  
289 distributions. The lognormal performed best or just as well as another model in 76.7% of the groups, the  
290 Weibull in 58.8%, the gamma in 35.2%, and the exponential in 25.7%. The lognormal model also fit 38.0% of  
291 groups better ( $> 2$  AIC units) than any of the other models. Whereas, the Weibull, gamma, and exponential  
292 models performed better than all others in 4.4%, 0.4%, and 0% of the groups, respectively.

293 With the lognormal model outperforming the other distributions, we sought to determine if the lognormal  
294 is objectively a good fit to the data. We used a Shapiro-Wilk's test of normality on the log-transformed  
295 data, after adjusting the p-values for multiple tests to account for false discovery rate (using the `p.adjust`  
296 function in R with method `fdr`). For 96.7% of sampled groups, we fail to reject the null hypothesis that the  
297 data follows a normal distribution (Fig. S3, at an adjusted significance level of  $\alpha = 0.05$ ). Cognizant that  
298 failure to reject the null is not proof of the null, we conclude there is not strong evidence that distributions  
299 deviate from a lognormal distribution.

### 300 **Question 2: Do patterns of aggregation in Bd intensity reflect biological pro-** 301 **cesses, such that there are quantifiable differences in aggregation between epi-** 302 **zoological states?**

#### 303 **Empirical results**

304 To gain mechanistic intuition on the broader results in this section, we first examined seven specific popula-  
305 tions from the Sierra dataset that 1) were repeatedly surveyed during Bd invasion and declines and 2) had  
306 sufficient samples of infected adults or subadults at a minimum of three time points to compute Poulin's  
307  $D$  ( $n \geq 2$ ). Fig. 3A shows the abundance trajectory of adult frogs in these populations through time,  
308 including the well-known pattern of dramatic population declines following Bd invasion. In Fig. 3B, we plot  
309 these same populations in intensity-aggregation space and see a consistent counterclockwise pattern emerge.  
310 Upon invasion, mean infection intensity is low, and aggregation is low. Once the population transitions to

311 the post-invasion phase, mean intensity is high, but aggregation remains relatively low. As the population  
312 progresses through the epizootic, mean intensity declines and aggregation increases. These patterns suggest  
313 that there is a signature of epizootic phase on observed patterns of aggregation.

314 To examine this pattern more broadly, we plotted 313 Sierra groups in intensity-aggregation space and  
315 observed a strong clustering of invasion, post-invasion, and enzootic groups (Fig. 4A-D) that was consistent  
316 with what we saw in our seven focal populations with time series data (Fig. 3B). Namely, the invasion stage  
317 was characterized by low mean intensity and low aggregation, the post-invasion phase was characterized  
318 by medium to high intensity and high to low aggregation, and the enzootic phase was characterized by  
319 intermediate mean intensity and high aggregation.

320 A distinct pattern that emerges in Fig. 4A-D is the notable unimodal shape of the data in intensity-  
321 aggregation space. The downward curvature is consistent with predictions from host-macroparasite theory  
322 that intensity-dependent mortality should reduce aggregation for high mean intensities as it truncates the  
323 tail of the Bd intensity distribution resulting in lower variance for a given mean within a population. This  
324 pattern was statistically supported by strong quadratic effect of mean intensity on aggregation, with the  
325 quadratic model performing better than the linear-effect only model ( $\Delta\text{AIC} = 150.13$  from comparing a  
326 model with quadratic effect to one with only a linear relationship). Moreover, this unimodal pattern was  
327 robust to different measures of aggregation (Fig. 4A-D).

328 Interestingly, putative enzootic populations rarely occupy the space of high mean intensity and low  
329 aggregation (Fig. 4). We observed seven enzootic populations in this region of high mean intensity and lower  
330 aggregation. Although one group in the enzootic stage was composed of adults, the rest were subadults—a  
331 life stage that still experiences substantial disease-induced mortality even in enzootic populations [45].

## 332 **Modeling results**

333 Modeling showed that the unimodal intensity-aggregation patterns likely contain important, mechanistic  
334 information about disease processes. The hump-shaped patterns in intensity-aggregation space found in the  
335 field data for all four metrics did not emerge trivially from the model; depending on parameter values, the  
336 model simulations produced this hump shape for none, some, or all metrics. Simulations with parameter  
337 values based mostly on laboratory experiments [19; 47] did not produce unimodal patterns for any of the  
338 four metrics (Fig S5), indicating different biological processes may occur in the field than in a lab setting.  
339 This possibility of a quantitative mismatch between the laboratory and the field is also supported by the  
340 observation that the laboratory-based parameter values produced significantly lower values of intensity and  
341 higher values of aggregation than was observed in the field. To address this possible mismatch, we explored  
342 additional parameter sets (details in supplementary material). When we weakened the negative density de-

pendence of pathogen growth within hosts and decreased the variance in initial infection load, our simulations produced slightly higher mean loads, lower aggregation, and a unimodal pattern in one metric, matching the field data somewhat better (Fig. S6). When we also decreased host mortality, parasite shedding rate (keeping prevalence from maxing out at one), and stochasticity in parasite growth, the model simulations produced higher intensities and still lower aggregation. Moreover, the model produced unimodal patterns for all four metrics (Fig. 4E-H). Thus, in terms of matching the intensity-aggregation patterns from the field, we considered this our best parameter set.

From host-macroparasite theory, we might expect that this unimodal pattern depends on intensity-dependent mortality driving lower aggregation at high intensity. Changing the parameter values so that hosts could survive very high loads with no mortality did increase aggregation somewhat, as expected, but unexpectedly did not significantly change the unimodal patterns (Fig. S8). Lastly, the path our simulation results take through intensity-aggregation space may explain observed counterclockwise motion through intensity-aggregation space for populations in Fig. 3B; if we sample our simulated populations at one month, one year, and thirty years to simulate the infrequent sampling of the field populations, we see how a counterclockwise motion could arise (e.g., colored points in Fig. 4E-H).

Our modeling further shows that the position of the enzootic populations in intensity-aggregation space may be a signal of host evolution. Host evolution of resistance that lowers pathogen growth rate moves populations left, toward lower mean intensity, and up, toward higher aggregation, in intensity-aggregation space for all four metrics (dashed black in Fig. 4E-H). This position of post-evolution populations higher and to the left of post-invasion populations that have experienced an epizootic but not yet evolved is consistent with the field data (Fig. 4). If hosts evolved a different defense, e.g., tolerance of higher parasite loads without dying, we would not observe this shift (Fig. S7). Thus, the enzootic populations' position in intensity-aggregation space may indicate the evolution of resistance rather than tolerance in the host.

## Discussion

Parasite aggregation is a strong driver of disease dynamics within host populations [20]. Though aggregation in macroparasites has been extensively examined, little has been done to systematically explore aggregation within host-fungal parasite systems, despite the known impact of fungal pathogen intensity on its host. In this study, we used a dataset of nearly 57,000 samples of amphibian infection intensity to show that i) Bd is consistently more aggregated than typical macroparasites, ii) the distribution of Bd intensity within a population is generally consistent with a lognormal distribution, and iii) patterns of Bd aggregation can contain consistent signatures of biological mechanisms. This study demonstrates the utility of fungal aggregation

374 as a means of identifying cryptic biological processes (e.g. disease-induced mortality or evolution of defense  
375 mechanisms) within host populations.

### 376 **Patterns of aggregation**

377 Although both macroparasites and fungal parasites are aggregated within hosts, the magnitude of aggrega-  
378 tion, as determined by the TPL slope, was significantly greater in Bd systems compared to many macropar-  
379 asites. There are two possible explanations for this result that we cannot separate in this study. First,  
380 because Bd can rapidly reinfect its hosts in a process akin to within-host reproduction, we would expect  
381 levels of aggregation to be higher than most macroparasites. Supporting this expectation, [28] demonstrated  
382 similar patterns of high aggregation in *Oxyuridae* pinworms that rapidly reinfect their host (TPL slope of  
383 *Oxyuridae* pinworms: 2.82 [2.44, 3.22]). For both pinworms and Bd, already-infected hosts can acquire  
384 additional infection faster than uninfected hosts, increasing the variance and skew in the distribution of  
385 parasites. Second, the values of the Bd TPL slopes were highly consistent across sites and host species, in-  
386 dicating that levels of aggregation are conserved across populations with widely varying biology. The highly  
387 conserved nature of aggregation in macroparasites can be partially explained through statistical constraints  
388 that are independent of parasite biology [e.g., 39; 3]. This might also be true for Bd. For example, given  
389 a lognormal distribution, we would expect a TPL slope of 2, generally consistent with what we observe  
390 across Bd systems. Lognormal distributions consistently emerge in dynamic population models in ecology  
391 [32] and it is possible that the lognormal distribution of Bd (and thus the TPL slope of 2) arises because  
392 Bd dynamics, swabbing, and testing are a combination of multiplicative random processes that necessarily  
393 lead to a lognormal distribution [i.e., a central limit theorem type of argument 48]. Regardless of the exact  
394 drivers, we found that Bd aggregation does not look like that of most macroparasites.

395 A major impetus for quantifying patterns of aggregation in host-parasite systems is to effectively build and  
396 analyze population-level models of host-parasite dynamics. In host-macroparasite systems, the application  
397 of the negative binomial distribution has led to many basic and applied ecological insights about host-  
398 macroparasite dynamics [20; 21; 49]. Models of fungal dynamics are adopting similar approaches to those  
399 of macroparasite modeling, focusing on modeling host infection intensity [17]. However, there are still few  
400 generalizable expectations regarding fungal distributions across hosts in a population, making subsequent  
401 model assumptions somewhat tenuous.

402 We found that distributions of Bd intensity, conditional on infection, were most consistent with lognormal  
403 distributions across species, life stages, and locations. Lognormal distributions describe the spatial distribu-  
404 tion of abundance and density of organisms in many natural systems and theoretically emerge in populations  
405 experiencing environmental and demographic stochasticity [32]. Surprisingly, the gamma distribution—the

406 continuous analogue to the negative binomial distribution—performed relatively poorly when describing Bd  
407 intensity distributions. As we continue to use models to describe observed fungal infection dynamics in  
408 the field, fitting empirical data to models generally requires making some distributional assumptions about  
409 fungal intensity. Currently, host-fungal models in amphibian-Bd systems have assumed that Bd intensi-  
410 ties are approximately lognormally distributed [50; 43], but this assumption has only been validated for  
411 a few focal amphibian-Bd systems. Our results show that a lognormal assumption is broadly applicable  
412 within amphibian-Bd systems, making theoretical and applied applications of these models robust across  
413 amphibian-Bd systems. While we only examined Bd in this study, we expect approximate lognormal distri-  
414 butions to hold more broadly across host-fungal systems. Testing this expectation is an important next step  
415 for uniting host-fungal dynamics under a common theoretical framework, as has been so successfully done  
416 with host-macroparasite dynamics.

### 417 **Mechanisms of aggregation**

418 While fungal aggregation was highly consistent across amphibian species and populations, we found that  
419 there are also distinct patterns that arise in fungal aggregation that reflect underlying biological processes.  
420 In the empirical data, we observed a notable reduction in aggregation in post-invasion populations that  
421 we know were experiencing high-levels of disease-induced mortality [based on previous field observations,  
422 15]. Moreover, we observed that the life stage in enzootic populations with the lowest levels of aggregation  
423 tended to be juveniles, the life stage in which disease-induced mortality is still occurring at a high rate  
424 even in enzootic populations [37]. While it is tempting to conclude that this pattern of reduced aggregation  
425 is solely driven by intensity-dependent mortality as predicted in host-macroparasite systems [2; 3], our  
426 modeling results show that reduced aggregation in post-invasion populations can arise even in the absence  
427 of intensity-dependent mortality.

428 The mechanism by which our model can produce the observed unimodal pattern in intensity-aggregation  
429 space is described as follows. When Bd first invades a population the observed intensity distribution is  
430 primarily structured by the dynamics of initial infection so that hosts have relatively similar low loads and  
431 low levels of aggregation. As the Bd outbreak proceeds, the distribution of fungal intensity begins to include  
432 both older infections with higher loads structured by within-host growth dynamics and newer infections  
433 with loads structured by initial infection dynamics. This mixture of newer and older infections increases  
434 aggregation in the intensity distribution. Most hosts become infected as the outbreak continues, and most  
435 infections are older and closer to the pathogen's within-host carrying capacity. This drives a subsequent  
436 increase in mean intensity and reduction in aggregation. Overall, the shift from mostly newer infections  
437 to a mixture of newer and older infections then finally to mostly older infections drive a unimodal pattern

438 in intensity-aggregation space. Our model shows that while we can get the expected unimodal pattern of  
439 reduced aggregation being driven predominantly by intensity-dependent mortality, the pattern requires that  
440 i) all hosts get infected essentially simultaneously and ii) hosts rarely lose infection during an outbreak.  
441 However, as these conditions are violated, the effect of intensity-dependent mortality on aggregation quickly  
442 becomes dwarfed by the joint effect of initial infection and within-host growth. Host-macroparasite theory has  
443 shown that there is not always a one-to-one mapping between aggregation patterns and biological processes  
444 [51]. Our results clearly highlight this point for fungal intensity distributions—there are two plausible  
445 biological mechanisms that could explain and jointly contribute to the observed reduction in aggregation at  
446 high loads: intensity-dependent mortality and the balance between initial infection and within-host growth  
447 along an epizootological trajectory. The latter is an aggregation mechanism that, to our knowledge, has not  
448 been considered in macroparasite systems, highlighting the need for unique theory describing the patterns  
449 and mechanisms of aggregation in host-fungus systems.

450 In addition to intensity-dependent mortality and the balance between initial infection and within-host  
451 growth, we found that patterns of aggregation contained clear signatures of the epizootological stage of a  
452 host-Bd system. Empirically, we saw populations follow a characteristic counterclockwise pattern on the  
453 yearly time scale in intensity-aggregation space. Interestingly, our modeling results illustrated that this  
454 counterclockwise pattern was likely a result of the timescale on which we observed these MYL frog-Bd  
455 systems. Our model showed that the transition from invasion phase to post-invasion epizootic phase should  
456 actually traverse a humped curve, rather than seamlessly jumping from the left to the right side of the  
457 curve. Because these sites were only sampled once a year, this data likely missed the transition from  
458 invasion phase ( $< 50\%$  prevalence) to post-invasion phase ( $> 50\%$  prevalence), as this often occurs rapidly  
459 within MYL frog-Bd systems. Therefore, we could only observe the invasion point and the post-invasion  
460 epizootic point within the intensity-aggregation space. Moreover, our model shows that the transition back  
461 to an intermediate intensity and high aggregation state does not occur in the model without some level of  
462 evolution in host defense; specifically, host evolution of resistance that lowers pathogen growth rate produced  
463 this pattern, while evolution of tolerance could not. MYL frog populations have persisted enzootically and  
464 begun to recover, likely due to evolved resistance to Bd [37]. As such, this is an intriguing basis for utilizing  
465 population-level aggregation patterns to identify biologically relevant processes in wild populations, such as  
466 the evolution of host defense.

467 Examining aggregation patterns in a system where epizootological phase was known a priori enabled us to  
468 discern patterns across the intensity-aggregation space. The full epizootological trajectory of many amphibian  
469 populations is rarely observed, and it is well known that similar amphibian populations infected with Bd  
470 can be at different places along an epizootological trajectory or on different trajectories altogether [52]. By

471 substituting spatial replication across populations for temporal replication within populations, we show that  
472 intensity-aggregation space can help locate disparate populations along a common epizootological trajectory.  
473 We expect the approach we develop to be particularly useful for species that are generally considered to be  
474 persisting enzootically with Bd, but in reality, may be experiencing cryptic invasions and epizootics across  
475 populations (e.g., Fig. S4).

## 476 **Conclusions**

477 Beyond amphibian-Bd systems, our study is useful for understanding fungal parasite dynamics in other  
478 wildlife populations. By extending our analyses to other host-fungal parasite systems, such as those involv-  
479 ing white-nose syndrome in bats or *B. salamandrivorans* in amphibians, we can elucidate broader patterns  
480 of aggregation of fungal parasites. This comparative approach can unveil commonalities and distinctions  
481 in fungal intensity patterns across different hosts and parasites. Identifying patterns of aggregation and  
482 how they reflect biological processes in diverse systems has implications for conservation strategies, dis-  
483 ease management, and disease modeling efforts. By demonstrating the ubiquity of aggregation, identifying  
484 distributional characteristics, and deciphering the biological significance of these patterns, we advance our  
485 understanding of host-fungal parasite ecology and pave the way for broader consideration of the implications  
486 of microparasite aggregation in wildlife disease ecology and epidemiological theory.

## 487 **Acknowledgements**

### 488 **Personnel and other acknowledgments**

489 We thank T. McDevitt-Galles, W. Moss, D. Calhoun, R. Chen, T. Riepe, K. Leslie, A. Barbella, K. Rose,  
490 Dan Wetzel, Aimee Danly, Caitlin Nordheim, Miranda Kosowsky, Laura A. Brannelly, Karie A. Altman,  
491 Renato A. Martins, J. Vargas Soto, E. Hegeman, and A. Lindauer and the many other individuals who  
492 helped with data collection, processing, management, and conceptual insights.

493 Institutes and organizations supporting this work were: University of Pittsburgh (IACUC Protocol  
494 #1602771); Vanderbilt University (IACUC #M1600250-0); UMass (IACUC #2014003); University of California-  
495 Santa Barbara; São Paulo Research Foundation (FAPESP propc #2021/10639-5); Brazilian National Council  
496 for Scientific and Technological Development (CNPq proc #304713/2023-6); Sierra Nevada Aquatic Research  
497 Laboratory; East Bay Regional Parks and Municipal Utility Districts; Santa Clara County Parks; Sequoia-  
498 Kings Canyon and Yosemite National Parks; Inyo and Sierra National Forests; Louisiana Department of

499 Wildlife and Fisheries (Scientific Research and Collecting Permits LNHP-17-029, LNHP-18-005, WDP-19-  
500 010); Pennsylvania Fish and Boat Commission; Tennessee Wildlife Resource Agency (Scientific Collection  
501 Permit #1546); Vermont Fish and Wildlife Department (Permit SR-2016-17); California Department of Fish  
502 and Wildlife; U.S. Fish and Wildlife Service; and multiple private landowners.

## 503 **Funding**

504 This project was supported by the National Park Service (to R.A.K.), Yosemite Conservancy (to R.A.K.), the  
505 US Fish and Wildlife Services Endangered Species Conservation and Recovery Grant Program, the National  
506 Science Foundation (EF-0723563, to C.J.B.; DEB-1557190, to C.J.B.; DEB-2133401, to M.Q.W.; and DBI-  
507 2120084, to C.L.R.Z., DBI-2120084, to RIBBiTR; DEB-2227340, to C.G.B.; IOS 2303908, to C.G.B.; DEB-  
508 2133401, to M.Q.W.; DEB-2133399, to T.C.S.; DEB-1149308; DEB-1754171), and the NIH/NSF Ecology and  
509 Evolution of Infectious Diseases program (R01GM109499 and R01GM135935).

## 510 References

- 511 [1] Poulin R. Are there general laws in parasite ecology? *Parasitology*. 2007 jun;134(Pt 6):763-76.
- 512 [2] Anderson RM, Gordon DM. Processes influencing the distribution of parasite numbers within host  
513 populations with special emphasis on parasite-induced host mortalities. *Parasitology*. 1982;85:373-98.
- 514 [3] Johnson PTJ, Wilber MQ. Biological and statistical processes jointly drive population aggregation :  
515 using host – parasite interactions to understand Taylor’s power law. *Proceedings of the Royal Society*  
516 *B*. 2017;284:20171388.
- 517 [4] Morrill A, Nielsen ÓK, Skírnisson K, Forbes MR. Identifying sources of variation in parasite aggregation.  
518 *PeerJ*. 2022;10:1-22.
- 519 [5] Lester RJG. A review of methods for estimating mortality due to parasites in wild fish populations.  
520 *Helgoländer Meeresuntersuchungen*. 1984 mar;37(1-4):53-64.
- 521 [6] Wilber MQ, Briggs CJ, Johnson PTJ. Disease’s hidden death toll: Using parasite aggregation patterns  
522 to quantify landscape-level host mortality in a wildlife system. *Journal of Animal Ecology*. 2020;89:2876-  
523 87.
- 524 [7] Shaw DJ, Dobson AP. Patterns of macroparasite abundance and aggregation in wildlife populations: a  
525 quantitative review. *Parasitology*. 1995 jan;111:111-33.
- 526 [8] Shaw DJ, Grenfell BT, Dobson AP. Patterns of macroparasite aggregation in wildlife host populations.  
527 *Parasitology*. 1998 dec;117:597-610.
- 528 [9] Anderson RM, May RM. Population biology of infectious diseases: Part I. *Nature*. 1979;280(2):361 367.
- 529 [10] Fisher MC, Henk DA, Briggs CJ, Brownstein JS, Madoff LC, McCraw SL, et al. Emerging fungal  
530 threats to animal, plant and ecosystem health. *Nature*. 2012 apr;484(7393):186-94.
- 531 [11] Langwig KE, Hoyt JR, Parise KL, Kath J, Kirk D, Frick WF, et al. Invasion dynamics of white-nose  
532 syndrome fungus, midwestern United States, 2012–2014. *Emerging Infectious Diseases*. 2015;21(6):1023-  
533 6.
- 534 [12] Lorch JM, Knowles S, Lankton JS, Michell K, Edwards JL, Kapfer JM, et al. Snake fungal disease: An  
535 emerging threat to wild snakes. *Philosophical Transactions of the Royal Society B: Biological Sciences*.  
536 2016;371(1709).

- 537 [13] Martel A, Blooi M, Adriaensen C, Van Rooij P, Beukema W, Fisher MC, et al. Recent introduction of  
538 a chytrid fungus endangers Western Palearctic salamanders. *Science*. 2014;346(6209):630-1.
- 539 [14] Scheele BC, Pasmans F, Skerratt LF, Berger L, Martel A, Beukema W, et al. Amphibian fungal  
540 panzootic causes catastrophic and ongoing loss of biodiversity. *Science*. 2019;363(6434):1459-63.
- 541 [15] Vredenburg VT, Knapp RA, Tunstall TS, Briggs CJ. Dynamics of an emerging disease drive large-  
542 scale amphibian population extinctions. *Proceedings of the National Academy of Sciences*. 2010  
543 may;107(21):9689-94.
- 544 [16] Langwig KE, Frick WF, Hoyt JR, Parise KL, Drees KP, Kunz TH, et al. Drivers of variation in species  
545 impacts for a multi-host fungal disease of bats. *Philosophical Transactions of the Royal Society B:  
546 Biological Sciences*. 2016;371(1709):20150456.
- 547 [17] Briggs CJ, Knapp RA, Vredenburg VT. Enzootic and epizootic dynamics of the chytrid fungal pathogen  
548 of amphibians. *Proceedings of the National Academy of Sciences of the United States of America*. 2010  
549 may;107(21):9695-700.
- 550 [18] Grogan LF, Phillott AD, Scheele BC, Berger L, Cashins SD, Bell SC, et al. Endemicity of chytridiomy-  
551 cosis features pathogen overdispersion. *Journal of Animal Ecology*. 2016;85(3):806-16.
- 552 [19] Wilber MQ, Langwig KE, Kilpatrick AM, McCallum HI, Briggs CJ. Integral Projection Models for host-  
553 parasite systems with an application to amphibian chytrid fungus. *Methods in Ecology and Evolution*.  
554 2016;7:1182-94.
- 555 [20] Anderson RM, May RM. Regulation and stability of host-parasite interactions: I. Regulatory processes.  
556 *Journal of Animal Ecology*. 1978;47(1):219-47.
- 557 [21] Rosà R, Pugliese A. Aggregation, stability, and oscillations in different models for host-macroparasite  
558 interactions. *Theoretical Population Biology*. 2002 may;61(3):319-34.
- 559 [22] Lester RJG, McVinish R. Does moving up a food chain increase aggregation in parasites? *Journal of  
560 the Royal Society, Interface*. 2016;13:20160102.
- 561 [23] Valenzuela-Sánchez A, Schmidt BR, Uribe-Rivera DE, Costas F, Cunningham AA, Soto-Azat C. Cryptic  
562 disease-induced mortality may cause host extinction in an apparently stable host-parasite system.  
563 *Proceedings of the Royal Society B: Biological Sciences*. 2017;284(1863).

- 564 [24] Hyatt AD, Boyle DG, Olsen V, Boyle DB, Berger L, Obendorf D, et al. Diagnostic assays and sam-  
565 pling protocols for the detection of *Batrachochytrium dendrobatidis*. *Diseases of Aquatic Organisms*.  
566 2007;73(3):175-92.
- 567 [25] Miller DAW, Talley BL, Lips KR, Campbell Grant EH. Estimating patterns and drivers of infection  
568 prevalence and intensity when detection is imperfect and sampling error occurs. *Methods in Ecology*  
569 *and Evolution*. 2012;3(5):850-9.
- 570 [26] DiRenzo GV, Campbell Grant EH, Longo AV, Che-Castaldo C, Zamudio KR, Lips KR. Imperfect  
571 pathogen detection from non-invasive skin swabs biases disease inference. *Methods in Ecology and*  
572 *Evolution*. 2018;9(2):380-9.
- 573 [27] Boyle DG, Boyle DB, Olsen V, Morgan JAT, Hyatt AD. Rapid quantitative detection of chytridiomycosis  
574 (*Batrachochytrium dendrobatidis*) in amphibian samples using real-time Taqman PCR assay. *Diseases*  
575 *of Aquatic Organisms*. 2004;60(2):141-8.
- 576 [28] Grear DA, Hudson P. The dynamics of macroparasite host-self-infection: a study of the patterns and  
577 processes of pinworm (*Oxyuridae*) aggregation. *Parasitology*. 2011 apr;138(5):619-27.
- 578 [29] Fowler AC, Hollingsworth TD. The dynamics of *Ascaris lumbricoides* infections. *Bulletin of Mathe-*  
579 *matical Biology*. 2016;78:815-33.
- 580 [30] Woodhams DC, Alford RA, Briggs CJ, Johnson M, Rollins-Smith LA. Life-history trade-offs influence  
581 disease in changing climates: Strategies of an amphibian pathogen. *Ecology*. 2008;89(6):1627-39.
- 582 [31] Johnson PTJ, McKenzie VJ. Effects of Environmental Change on Helminth Infections in Amphibians:  
583 Exploring the Emergence of *Ribeiroia* and *Echinostoma* Infections in North America. In: Fried B,  
584 Toledo R, editors. *The Biology of Echinostomes*. New York: Springer Science+Business Media; 2008. p.  
585 249-80.
- 586 [32] Lande R, Engen S, Saether BE. *Stochastic Population Dynamics in Ecology and Conservation*. Oxford:  
587 Oxford University Press; 2003.
- 588 [33] Longo AV, Rodriguez D, da Silva Leite D, Toledo LF, Mendoza Almeralla C, Burrowes PA, et al. ITS1  
589 copy number varies among *Batrachochytrium dendrobatidis* strains: implications for qPCR estimates of  
590 infection intensity from field-collected amphibian skin swabs. *PloS One*. 2013;8(3):e59499-9.
- 591 [34] Byrne AQ, Waddle AW, Saenz V, Ohmer M, Jaeger JR, Richards-Zawacki CL, et al. Host species is  
592 linked to pathogen genotype for the amphibian chytrid fungus (*Batrachochytrium dendrobatidis*). *PLoS*  
593 *ONE*. 2022;17(3 March):1-17.

- 594 [35] Kilpatrick AM, Ives AR. Species interactions can explain Taylor's power law for ecological time series.  
595 Nature. 2003;19(1990):65-8.
- 596 [36] Lagrue C, Poulin R, Cohen JE. Parasitism alters three power laws of scaling in a metazoan commu-  
597 nity: Taylor's law, density-mass allometry, and variance-mass allometry. Proceedings of the National  
598 Academy of Sciences. 2015;112(6):1791-6.
- 599 [37] Knapp RA, Wilber MQ, Byrne AQ, Joseph MB, Smith TC, Rothstein AP, et al. Evolutionary rescue  
600 and reintroduction of resistant frogs allows recovery in the presence of a lethal fungal disease. bioRxiv.  
601 2023. Available from: <https://www.biorxiv.org/content/early/2023/05/24/2023.05.22.541534>.
- 602 [38] Duerr HP, Dietz K. Stochastic models for aggregation processes. Mathematical Biosciences.  
603 2000;165(2):135-45.
- 604 [39] Wilber MQ, Johnson PTJ, Briggs CJ. When can we infer mechanism from parasite aggregation? A  
605 constraint-based approach to disease ecology. Ecology. 2017;98(3):688-702.
- 606 [40] Gaba S, Ginot V, Cabaret J. Modelling macroparasite aggregation using a nematode-sheep system:  
607 the Weibull distribution as an alternative to the Negative Binomial distribution? Parasitology. 2005  
608 apr;131(03):393.
- 609 [41] Poulin R. The disparity between observed and uniform distributions: A new look at parasite aggregation.  
610 International Journal for Parasitology. 1993;23(7):937-44.
- 611 [42] McVinish R, Lester RJG. Measuring aggregation in parasite populations. Journal of the Royal Society  
612 Interface. 2020;17(165):20190886.
- 613 [43] Wilber MQ, Ohmer MEB, Altman KA, Brannelly LA, LeSage EH, LaBumbard BC, et al. Once a  
614 reservoir, always a reservoir? Seasonality affects the pathogen maintenance potential of amphibian  
615 hosts. Ecology. 2022;103:e3759.
- 616 [44] Zhou H, Hanson T, Knapp R. Marginal Bayesian nonparametric model for time to disease arrival of  
617 threatened amphibian populations. Biometrics. 2015;71(4):1101-10.
- 618 [45] Knapp RA, Fellers GM, Kleeman PM, Miller DA, Vredenburg VT, Rosenblum EB, et al. Large-scale  
619 recovery of an endangered amphibian despite ongoing exposure to multiple stressors. Proceedings of  
620 the National Academy of Sciences. 2016;113:11889-94.

- 621 [46] Wilber MQ, Knapp RA, Smith TC, Briggs CJ. Host density has limited effects on pathogen invasion,  
622 disease-induced declines and within-host infection dynamics across a landscape of disease. *Journal of*  
623 *Animal Ecology*. 2022;(May):2451-64.
- 624 [47] Wilber MQ, Knapp RA, Toothman M, Briggs CJ. Resistance, tolerance and environmental transmis-  
625 sion dynamics determine host extinction risk in a load-dependent amphibian disease. *Ecology Letters*.  
626 2017;20:1169-81.
- 627 [48] McGill BJ, Nekola JC. Mechanisms in macroecology: AWOL or purloined letter? Towards a pragmatic  
628 view of mechanism. *Oikos*. 2010 apr;119(4):591-603.
- 629 [49] Hudson PJ, Dobson aP, Newborn D. Prevention of population cycles by parasite removal. *Science (New*  
630 *York, NY)*. 1998;282(5397):2256-8.
- 631 [50] Wilber MQ, Pfab F, Ohmer MEB, Briggs CJ. Integrating infection intensity into within- and between-  
632 host pathogen dynamics: implications for invasion and virulence evolution. *The American Naturalist*.  
633 2021;198(6):661-77.
- 634 [51] Duerr HP, Dietz K, Eichner M. On the interpretation of age-intensity profiles and dispersion patterns  
635 in parasitological surveys. *Parasitology*. 2003 jan;126(1):87-101.
- 636 [52] Jani AJ, Knapp RA, Briggs CJ. Epidemic and endemic pathogen dynamics correspond to distinct host  
637 population microbiomes at a landscape scale. *Proceedings of the Royal Society B*. 2017;284:20170944.

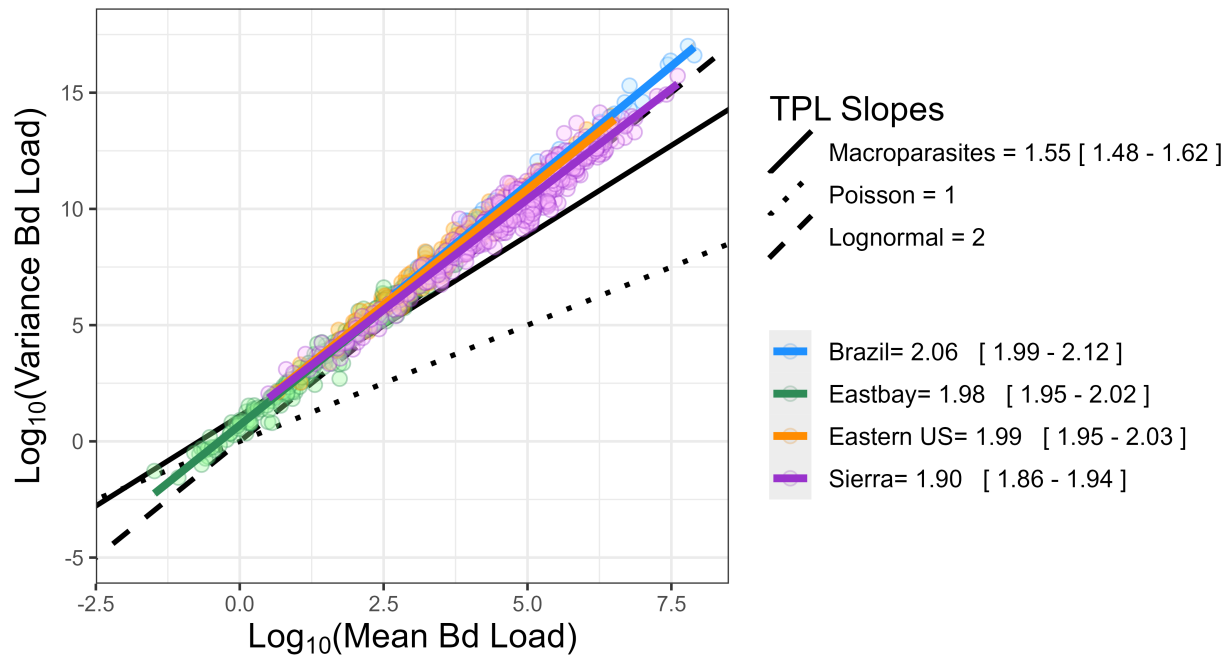


Figure 1: The relationship of log mean and log variance of fungal intensity for all groups. Regression lines were fit to each dataset. Slopes and their 95% confidence intervals are provided in the legend. The solid black line represents the slope that is typically seen in macroparasites (1.55, 95% CI [1.48-1.62] ) [7]. The dotted line with a slope of 1 is expected in a Poisson distribution (null distribution for macroparasites) and the dashed line with a slope of 2 is expected for a lognormal distribution.

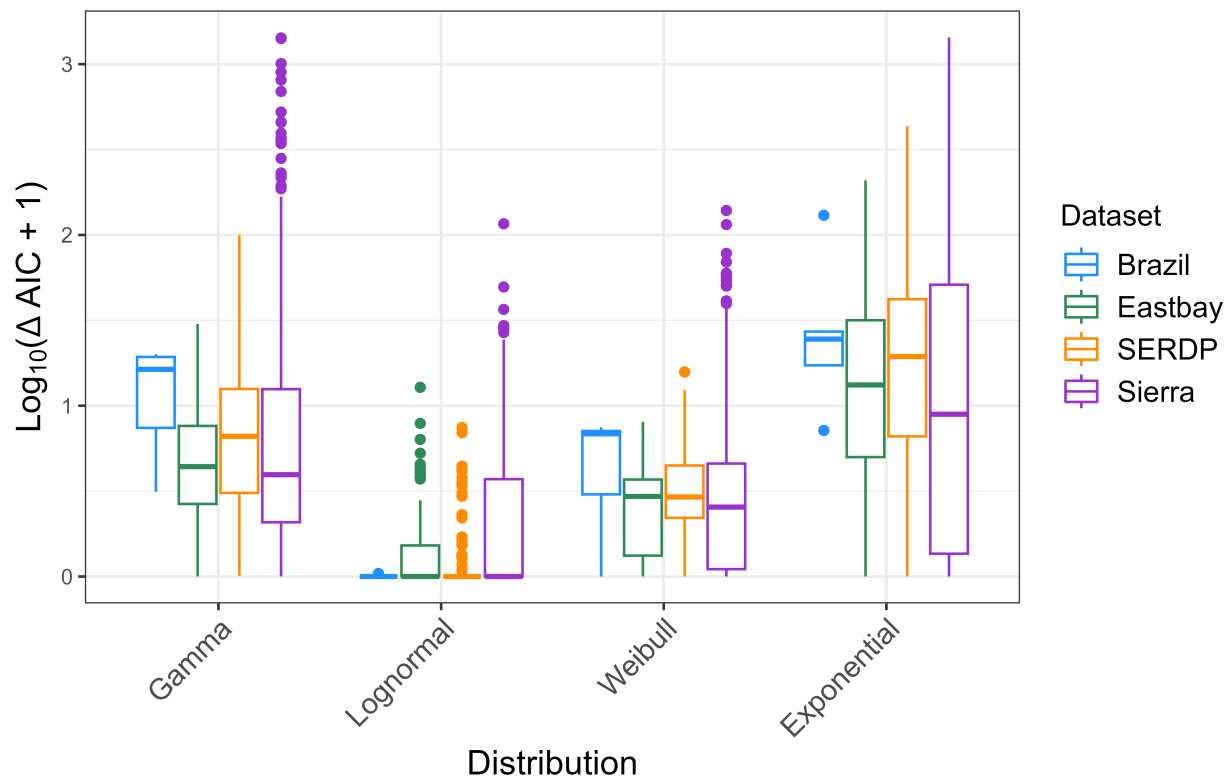


Figure 2: Comparison of  $\log_{10}(\Delta AIC + 1)$  values across the four continuous distributions that were fit to the fungal intensity data for the 525 amphibian groups across four datasets. Each data point was a group of amphibians that had at least 10 infected individuals.

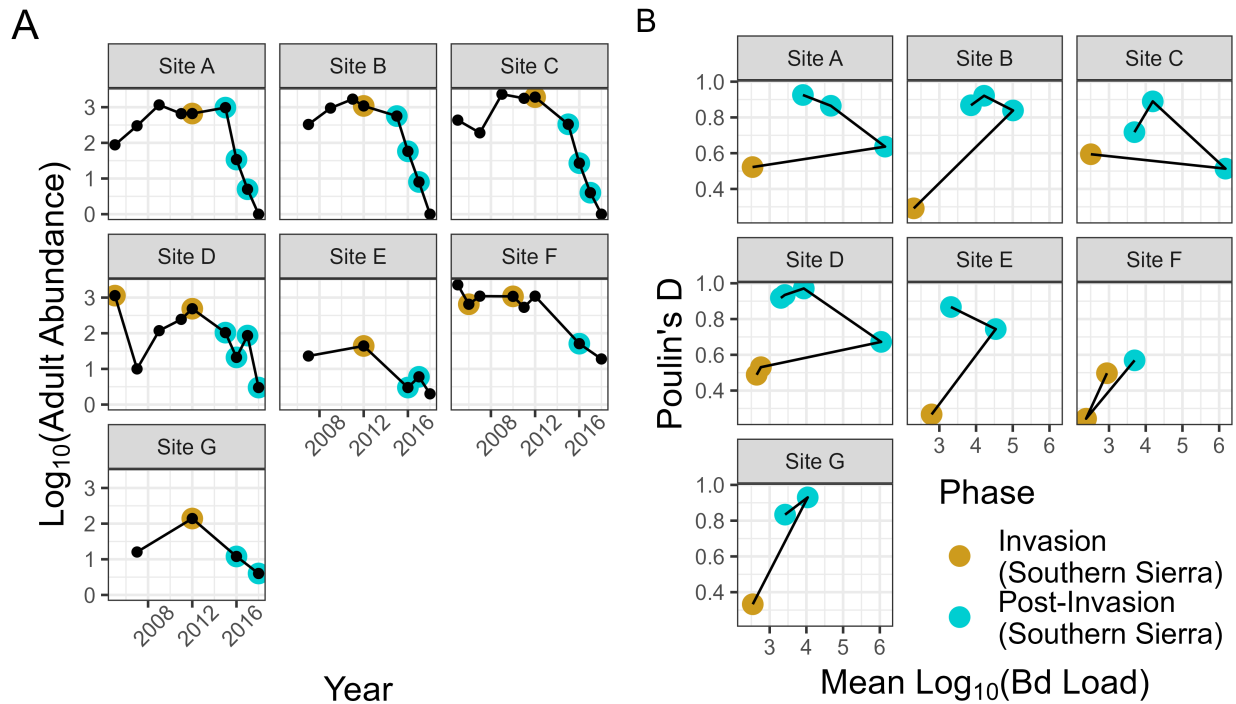


Figure 3: **A.** The adult abundance trajectories of seven focal MYL frog populations through time. Black points show each time the population was surveyed for abundance and Bd and colored points indicate when a sufficient number of infected individuals ( $n \geq 2$ ) were sampled to compute Poulin's D, with a higher value indicating more aggregation. The invasion phase was delineated when prevalence was less than 0.5, following Wilber et al. (2022) [46]. **B.** The same seven populations with trajectories plotted in intensity-aggregation space. The colored dots in B. correspond to the same colored dots in A.

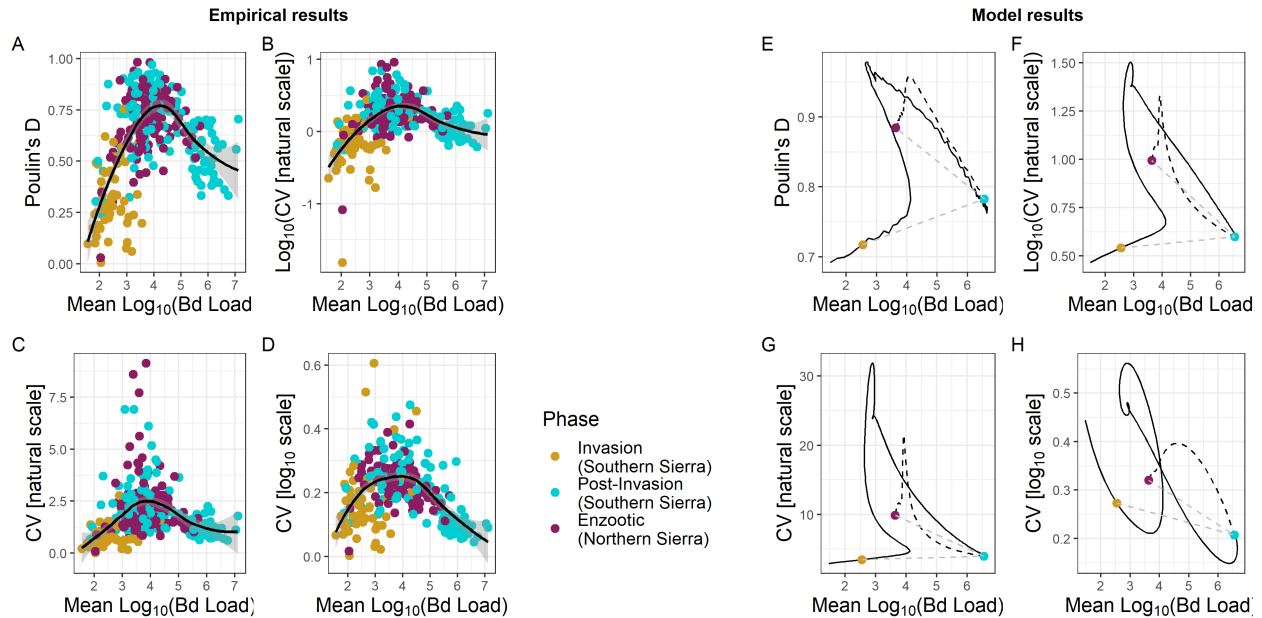


Figure 4: Groups in different epizootological phases plotted as a relationship between mean log<sub>10</sub> Bd intensity and different aggregation metrics. **A.** Soon after Bd invasion, mean loads and aggregation (Poulin's D) are low (yellow points). Later, post-invasion, mean loads are high and aggregation is still relatively low (blue points). Then much later, mean loads are intermediate and aggregation is higher (purple points), leading to an overall unimodal shape. This same pattern holds for other aggregation metrics including **B.** log<sub>10</sub> of CV (coefficient of variation) on the natural scale, **C.** CV on the natural scale, and **D.** CV on the log<sub>10</sub> scale. The unimodal trend for all empirical results is emphasized through a best-fit spline (black). The shaded gray region is the 95% confidence interval around the best fit spline. A parameterized IPM model can generally reproduce these hump-shaped patterns in all four metrics without evolution (black curve in **E-H**); we compare empirical to model results for each metric as the model need not necessarily produce a hump shape in every metric (e.g., see Fig. S5, S6). Evolution of lower pathogen growth rate (dashed black) moves populations to lower mean loads and higher aggregation metrics, generally matching the empirical results for enzootic populations. We plot the points corresponding to sampling the model results at one week (invasion, yellow), one year (post-invasion, blue), and thirty-one years (enzootic, purple) for comparison to the empirical results in Fig. 3B; low temporal resolution sampling can create a counterclockwise pattern in intensity-aggregation space (emphasized by dotted gray line connecting colored points in **E-H**).